Evidence of Jovian active longitude: 3. Observational constraints

Patrick H. M. Galopeau, M. Y. Boudjada

Evidence of Jovian active longitude: 3. Observational constraints

P. H. M. Galopeau[1] and M. Y. Boudjada[2]

Received 14 May 2010; revised 20 August 2010; accepted 17 September 2010; published 9 December 2010.

[1] The occurrence probability of the Io-controlled Jovian decameter radio emissions depends on the central meridian longitude and the orbital phase of the satellite Io. Investigations by Galopeau et al. (2004, 2007) have shown that some specific Jovian "active" longitudes favor the radiation. The authors proposed a model which involves the cyclotron maser instability (CMI) as the mechanism at the origin of the Jovian radio emissions produced near the local gyrofrequency, along an active magnetic field line carried away by Io through its revolution around Jupiter. Those studies brought out the existence of an active longitude anchored in Jupiter's magnetic field and directly related to the efficiency of the CMI. In the present analysis, we model the four occurrence regions associated to Io-controlled sources. This approach is in a reverse way of the parametric method developed by Galopeau et al. (2007). The properties of the propagation and polarization of the radio wave, derived from the CMI, are the key ingredients for the study of the beaming cone. It is shown that the lead angle of the active magnetic field line relative to Io has a significant effect on both the selection of the propagation conditions and the limit between the right- and left-hand polarization states. The modeled and observed occurrence regions are found to be similar for a lead angle of about 20°. However, it seems that the behaviors of the southern and northern sources are not alike despite a common generation mechanism.

Citation: Galopeau, P. H. M., and M. Y. Boudjada (2010), Evidence of Jovian active longitude: 3. Observational constraints, *J. Geophys. Res.*, *115*, A12221, doi:10.1029/2010JA015677.

1. Introduction

[2] Jovian decametric (DAM) radio emissions were discovered more than a half century ago by *Burke and Franklin* [1955]. It is considered a precursor for the study of planetary radio auroral radiations, and the dynamic interaction of a satellite, like Io, with the magnetized environment of the planet. More details about the phenomenology and morphology of the Jovian DAM emission were reported in two books by *Carr and Desch* [1976] and *Carr et al.* [1983]. However, several questions are addressed when one tries to confront the generation mechanism, the cyclotron maser instability (CMI) [*Wu and Lee*, 1979] with the Jovian DAM ground-based observations.

1.1. The 50 Years of DAM Ground-Based Observations

[3] A regular monitoring of the Jupiter auroral emissions by ground-based stations leads us to find repetitive and recurring observational features, which can be related to the magnetospheric physics of the planet and its particular interaction with the satellite Io.

1.1.1. CML-Io Phase Diagram

[4] The long-term ground observations show that the occurrence probability of the DAM radiation depends on two essential parameters: the central meridian longitude (CML, System III), which is linked to the internal rotating magnetic field of Jupiter, and the orbital phase of the satellite Io. The CML-Io phase diagram, which displays the occurrence of the emission as a function of the CML and the Io phase, reveals several zones of enhanced occurrence probability which have been named Io-controlled sources: Io-A, Io-B, Io-C, and Io-D. The occurrence probability is defined as the ratio of the time durations of the emission to the time duration of the observation as shown by *Leblanc et al.* [1993a] in the case of the Nançay decametric array in France [*Lecacheux*, 2000]. The area occurrence size and the position of these "sources" in the CML-Io phase diagram mainly depend on the observation frequency [*Genova and Aubier*, 1987] and on the period of about 12 years where the Jovicentric declination of the Earth changes from −3.5° to + 3.5° [*Boudjada and Leblanc*, 1992]. One should add to these previous parameters the observation constraints which are limited to a maximum of 8 h per day (4 h before and after the local meridian transit of the planet) and also the change in observing frequency range due to variable, daily, and seasonal ionospheric propagation conditions. The latter are optimal in winter when

[1]LATMOS, Université Versailles Saint-Quentin-en-Yvelines, CNRS, INSU, IPSL, Guyancourt, France.
[2]Space Research Institute, Austrian Academy of Sciences, Graz, Austria.

0148-0227/10/2010JA015677

the transit meridian of the planet is close to midnight local time [*Aubier et al.*, 2000].

1.1.2. Arc Structures in Jovian DAM Emissions

[5] Radio receivers with a large-frequency bandwidth (from 10 MHz to 40 MHz) enables us to record the dynamic spectrum of the DAM emissions, which displays the variation of the intensity level versus the observation time and the frequency. The main component of the Jovian decametric radiations appears as arc shapes which have been classified in two groups: the so-called vertex early arcs (VEA) and vertex late arcs (VLA). The curvatures of the arcs are the result of the emission diagram which is supposed to be a hollow cone [*Dulk*, 1965]. The conventional model groups sources by pairs, like {Io-A, Io-B} or {Io-C, Io-D}, as two sides of a same hollow cone [*Carr et al.*, 1983]. Sources which belong to the same hollow cone are then supposed to be emitted from the same hemisphere: {Io-A, Io-B} and {Io-C, Io-D} are radiated from the northern and southern hemispheres, respectively. The Jovian DAM emission is also right- and left-hand elliptically polarized [*Lecacheux et al.*, 1991]. Geometrical models have been proposed to explain the shape of the arcs taking into consideration the opening angle of the hollow cone, the magnetic field model of Jupiter [*Connerney*, 1992, 1993; *Connerney et al.*, 1998; *Grodent et al.*, 2008], and the emission at the gyrofrequency [*Lecacheux et al.*, 1998, and references therein].

1.1.3. Open Questions

[6] The CMI is usually accepted to be at the origin of Jovian decametric emissions, but also responsible for the auroral emissions related to magnetized planets like the Earth and Saturn. Despite long-term observations of Jovian DAM emissions, the confrontation between this generation mechanism and observations has not yet been worked on in depth. All these radiations are produced in mediums presenting very similar characteristics for their electron distribution function in energy and velocity (see review by *Treumann* [2006]). However, a detailed analysis of those radio emissions is far from being understandable, particularly regarding the spectral features (fine structures, narrow- and broadband emissions), the emission occurrence, and the produced diagram of emission.

1.2. Jovian Active Longitude

[7] Two approaches have been proposed with the aim of explaining the CML-Io phase diagram, in particular, the dependence of the source occurrence on the central meridian longitude [*Galopeau et al.*, 2004, 2007; *Zaitsev et al.*, 2005, 2006]. Their authors based their respective studies on theoretical models involving, on the one hand, the efficiency of the CMI in Jupiter's ionosphere and, on the other hand, the electron acceleration mechanism in the vicinity of Io. In the following we detail these two approaches.

[8] Other publications have reported the relationship between the morphology aspects of the DAM emissions and a hollow cone beam. They are based on the study of modulation lanes in the dynamic spectra of the radiation [see *Imai et al.*, 2002, and references therein]. In a recent paper, using data of the Cassini radio and plasma wave science (RPWS) experiment, *Imai et al.* [2008] studied the localization of the active magnetic flux tubes of the non-Io-B and non-Io-A sources.

1.2.1. Efficiency of the Cyclotron Maser Instability

[9] Theoretical evidence of Jovian active longitude was provided, in the first paper, by *Galopeau et al.* [2004]. The authors supposed that the occurrence probability of the radiation was linked to the amplification efficiency of the radio waves by the CMI. Hence, it was relevant to numerically work out the maximum growth rate of the CMI, assuming the radiation was emitted at the gyrofrequency along an active magnetic field line. Two maxima of the growth rate were found at two specific longitudes: ~130° and ~200° corresponding to a DAM radiation coming from the northern and southern hemispheres, respectively. They define the centers of the active longitude range, the location of which is mainly governed by the variation of the magnetic field gradient ∇B at the footprint of the active field line. This investigation leads, for the first time, to the production of a "simulated" CML-Io phase diagram based on the following conditions: (1) the active magnetic field line must cross the CMI active domain rotating with Jupiter and, (2) at the same time, the observer at the Earth's orbit must intersect the hollow cone representing the beaming of the radiation. This first paper [*Galopeau et al.*, 2004] provides evidence that the CMI generates active longitude ranges anchored in the planet.

[10] In the second paper [*Galopeau et al.*, 2007], a parametric approach was considered by taking into consideration the effect of observational parameters on the source occurrence in the simulated CML-Io phase diagram. Four parameters were regarded as key factors: the lead angle of the active magnetic field line relatively to Io, the declination of the Earth, the half angle of the emission cone, and the frequency of the radiation. A similarity was found between the observed and the simulated CML-Io phase diagram, in particular, when the lead angle is equal to 40°. In this case, the sources are localized in their correct occurrence regions as observed during the Voyager encounters with Jupiter [*Genova and Aubier*, 1987]. Also the absence of left-hand polarized emission at a frequency higher than 24 MHz is also predicted by this model, since those emissions are expected to emanate from the southern hemisphere. Despite this agreement between the simulated and the observed CML-Io phase diagram, the authors pointed out the impossibility of simultaneously fitting the correct occurrence areas of the four Io-controlled sources. One needs to change a specific parameter to place the source to its correctly observed position. *Galopeau et al.* [2007] concluded that the active longitude (mainly linked to the magnetic field of Jupiter) is not the only factor determining the occurrence probability.

1.2.2. Acceleration of Particles in Io's Ionosphere

[11] An alternative idea was proposed by *Zaitsev et al.* [2005, 2006], totally unlike the work by *Galopeau et al.* [2007], explains the dependence of the Io-related DAM emission on the CML. This study is based on the occurrence probabilities derived from Voyager observations as reported by *Aubier and Genova* [1985]. The authors show that this dependence is due to the existence of "active longitudes" by Io's orbit. Their active longitudes are the result of two antagonistic factors: a particle acceleration in Io's ionosphere produced by the motion of Io across the Jovian magnetic field and a pitch angle scattering of the accelerated electrons caused by interaction with plasma waves and whistlers when they travel through the Io plasma torus. Both acceleration and pitch angle scattering depend on the longitude of Io because the equatorial magnetic field of Jupiter is not constant and also because the Io plasma torus is located in the centrifugal equator which forms an angle of ~7° with the plane of Io's

Table 1. Limits of the Rectangular Source Boxes[a]

Source	CML 1	Io Phase 1	CML 2	Io Phase 2
A	204°	180°	265°	254°
B	90°	66°	204°	110°
C	299°	221°	33°	254°
D	0°	90°	204°	110°

[a]Each source in the CML-Io phase diagram is modeled as a rectangle box, the lower left corner (upper right corner) of which is defined by CML 1 and Io Phase 1 (CML 2 and Io Phase 2).

orbit. *Zaitsev et al.* [2003] proposed a mechanism for the acceleration of electrons in Io's ionosphere. They showed that the motion of the satellite across Jupiter's magnetic field induces a perpendicular electric field in its ionosphere, proportional to the velocity of Io relative to the corotating magnetospheric plasma and unable to accelerate particles. Because of the anisotropy of conductivity in Io's ionosphere, the induced electricfield tends to generate Hall currents orthogonal to the satellite surface which cannot close and which then lead to a strong charge separation. The electric field resulting from this charge separation presents a component parallel to the magnetic field, able to accelerate electrons up to energies of ~100 keV. Before reaching the source region of the radio emission located in Jupiter's ionosphere, the accelerated electrons must cross the Io plasma torus where their pitch angle is scattered. As a consequence, only part of those electrons reach the source zone, their flux is all the weaker as they travel through a thicker plasma region. *Zaitsev et al.* [2006] found that the most effective acceleration occurs in the longitude range $120° \leq \lambda_{Io} \leq 300°$, which is in agreement with the Io active longitude derived from Voyager observations, mainly associated with the northern hemisphere.

1.3. Aim of the Present Paper

[12] In this new study, we attempt to complete the investigation developed in the two previous papers [*Galopeau et al.*, 2004, 2007]. Our aim is to find the correct observational parameters which lead to the right fit of the observed CML-Io phase diagram, taking into consideration the source occurrence regions of the Io-controlled sources. This approach is the opposite of that used in the parametric analysis investigated by *Galopeau et al.* [2007]. In section 2, we describe the applied method to produce the modeled CML-Io phase diagram and the way to constraint it from the observed one. In section 3, we summarize the main results and we discuss principally the insufficiencies of models based on simple CMI application to explain the observed occurrence associated to the Jovian Io-controlled emissions. In section 4, we address some issues which present a real difficulty to finding an agreement between the observed and the modeled CML-Io phase diagram.

2. Reversal of Parametric Studies

[13] In this section, we describe the different steps we use to define specific rectangular "boxes" (in CML and Io phase) which delimit the occurrence regions of the Io-controlled sources as derived from observations of Jovian decametric radio emissions.

2.1. Source Occurrence Regions and Active Longitude Model Assumptions

[14] The first step consists of characterizing and identifying the occurrence regions in the CML-Io phase diagram for the four Io-controlled sources. We use the Jovian decametric observations recorded by the Nançay (France) and Boulder (USA) radio stations which covered a period of more than 20 years [*Genova et al.*, 1989]. We define rectangles associated with the occurrence regions of Io-controlled emissions, two emitted from the northern hemisphere (Io-A and Io-B) and the others from the southern one (Io-C and Io-D). Table 1 lists the limits for each source (in CML and Io phase) of this rectangle. It is important to remind here that the occurrence regions depend on some observational parameters as discussed in details by *Galopeau et al.* [2004]. However, we select for each source the rectangle in which most of the occurrence is detected.

[15] In the second step, we consider the physical hypotheses which have been applied to derive the active longitude ranges [see *Galopeau et al.*, 2004, 2007]. We recall hereafter the main hypotheses: (1) Electrons are accelerated in the neighborhood of Io's wake and follow an adiabatic motion along an active magnetic field line shifted by an angle δ relative to Io. (2) Electrons disappear by collision in Jupiter's ionosphere leading to a loss cone distribution function supposed to be the source of free energy needed by the CMI to produce the radiation. (3) The radiation, generated by the CMI, is emitted at the local gyrofrequency within a hollow cone of half angle θ, the axis of which is parallel to the local magnetic field vector **B**.

[16] Figure 1 shows a schematic illustration of the location of the Io-controlled sources in both hemispheres. For each source, we have indicated the hollow cone with the corresponding opening angle θ and the associated active field line. The Jovian magnetic field vector is outward (inward) in

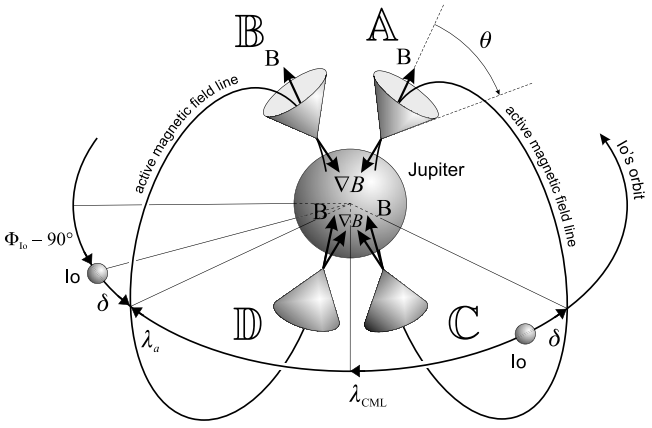

Figure 1. Schematic illustration of the parameters needed for the description of the Io-controlled DAM emission. The radiation is supposed to be emitted at the local gyrofrequency along an active magnetic field line intersecting Io's wake with a lead angle δ. The radio emission is beamed into a hollow cone with half angle θ and axis parallel to the direction of the local magnetic field **B** (or gradient of the magnetic field modulus ∇B).

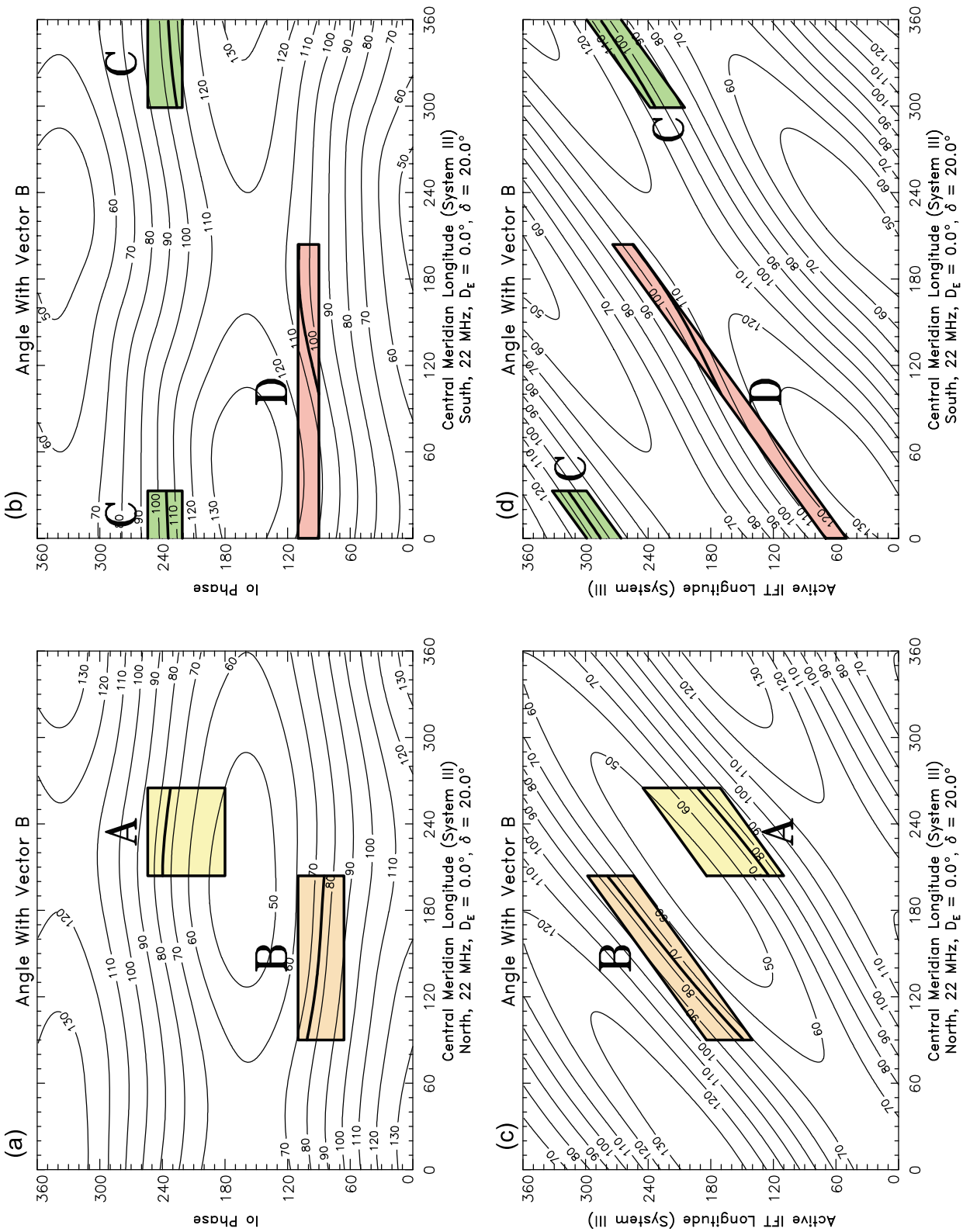
(a)
Angle With Vector B
Io Phase
Central Meridian Longitude (System III)
North, 22 MHz, D_E = 0.0°, δ = 20.0°
A
B
(b)
Angle With Vector B
Io Phase
Central Meridian Longitude (System III)
South, 22 MHz, D_E = 0.0°, δ = 20.0°
C
D
(c)
Angle With Vector B
Active IFT Longitude (System III)
Central Meridian Longitude (System III)
North, 22 MHz, D_E = 0.0°, δ = 20.0°
A
B
(d)
Angle With Vector B
Active IFT Longitude (System III)
Central Meridian Longitude (System III)
South, 22 MHz, D_E = 0.0°, δ = 20.0°
C
D

Figure 2

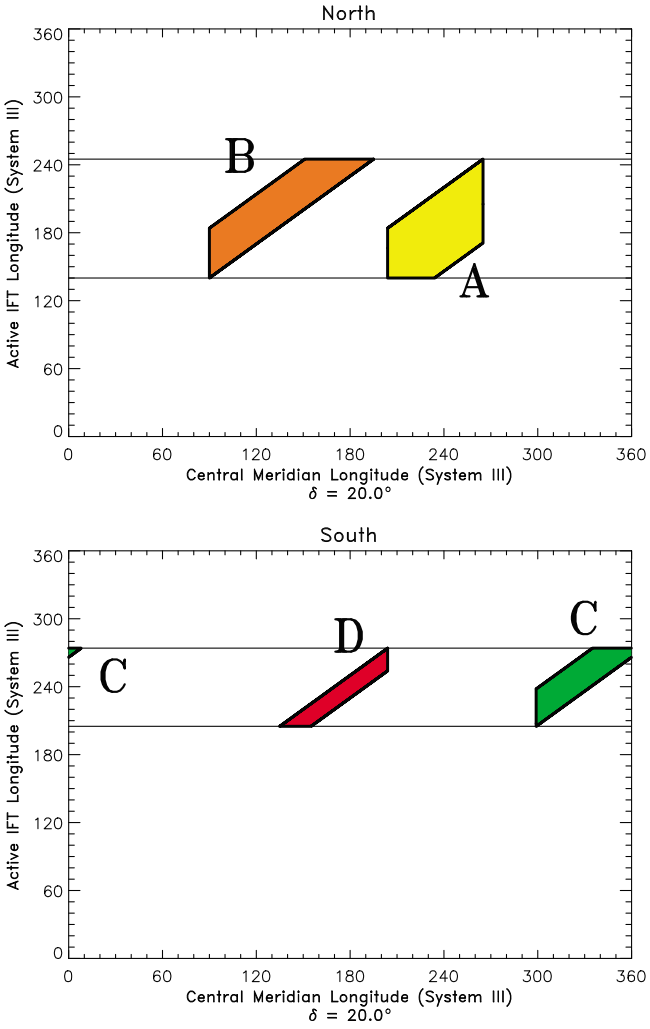

Figure 3. (top) Only the parts of the northern sources Io-A and Io-B corresponding to a common "active Io flux tube" longitude range have been displayed. (bottom) The same processing is applied to the southern sources Io-C and Io-D. We make the hypothesis that a same active longitude flux tube is at the origin of the emissions from both sources A and B (C and D). The resulting Jovian active longitude range is 140°–245° for the northern hemisphere and 205°–274° for the southern hemisphere for a lead angle $\delta = 20°$.

the northern (southern) hemisphere, whereas the magnetic field gradient ∇B is always inward. As indicated in Figure 1, in the planetary equatorial plane, we define the following angles: the (westward System III) central meridian longitude λ_{CML}, the (westward System III) longitude λ_a of the active magnetic field line, its (eastward) lead angle δ, and the (eastward) Io phase Φ_{Io}. These angles are linked together by the following relation:

$$\lambda_a = \lambda_{CML} + \pi - \Phi_{Io} - \delta. \quad (1)$$

Those parameters are used as ingredients to attempt to fit the observed occurrence regions.

2.2. Observational Constraint on Active Longitude Range

[17] First, we start to find a unique active longitude range which can fit the emission coming from each hemisphere. Figures 2a and 2b show a contour plot of the angle between the direction of the observer (located on the Earth) and the local magnetic field vector **B** deduced from the O6 model [*Connerney*, 1992, 1993] as a function of the CML and Io phase. The contours are displayed for each hemisphere (north and south), for a frequency equal to 22 MHz, a lead angle of 20°, and a Jovicentric declination of the Earth equal to 0°. Each contour represents a constant value of the opening angle θ of the emission cone. We also indicate the Io-controlled source regions by rectangular boxes, the limits of which are given in Table 1. The pairs {Io-A, Io-B} and {Io-C, Io-D} are supposed to be emitted from the northern and southern hemispheres, respectively. It is clear from Figures 2a and 2b that several values of θ are possible for the same source and that a thickness $\Delta\theta$ is required for the emission cone. The thick line inside each box corresponds to the portion of the beaming cone intercepting the source region, average values of 75° and 105° have been found for the angle θ in the north and south, respectively. Figures 2c and 2d show the same contours and source boxes versus the CML and the active Io flux tube (IFT) longitude. Equation (1) has been used to make the transformation from Φ_{Io} to λ_a. One can see from Figure 2 that, in each hemisphere, the two sources of the same pair do not spread over a unique range of active longitude.

[18] For each of the two pairs, {Io-A, Io-B} and {Io-C, Io-D}, we determine the active IFT longitude range shared by both sources. Figure 3 displays, for each hemisphere, the parts of the sources corresponding to this common active longitude range, the limits of which are indicated by two horizontal lines. We assume that a unique active zone (of Jovian longitude) triggers the radio emissions of the two sources in each hemisphere (Io-A and Io-B in north, Io-C and Io-D in south). In the case $\delta = 20°$ (Figure 3), the two active longitude ranges are 140°–245° and 205°–274° in the northern and southern hemispheres, respectively. It is noteworthy to mention that the active longitude range of the northern sources is more extended than that of the southern ones, as a consequence the Io-D source is limited to a narrow active longitude range.

Figure 2. (a and b) Angle between the direction of the observer (located on the Earth) and the local magnetic field vector **B** (from O6 model) in the source as a function of the central meridian longitude (System III) and the Io phase in northern (Figure 2a) and southern (Figure 2b) hemispheres. The boxes labeled A, B, C, D correspond to the well-known Io-controlled sources. The thick lines inside the boxes correspond to the portion of the beaming cone (with half angle $\theta = 75°$ for the north and $\theta = 105°$ for the south) fitting into the sources. (c and d) The same angle and boxes (A, B, C, D) are displayed as a function of the observer's longitude and the active Io flux tube longitude. A lead angle $\delta = 20°$ is used in this study.

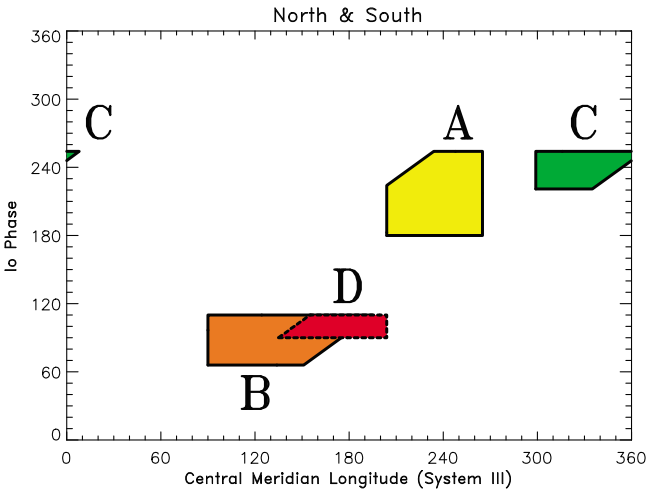

Figure 4. The four sources A, B, C, and D derived from Figure 3 are plotted versus the central meridian longitude and Io phase. This layout corresponds to a radiation produced by a unique active longitude range in each hemisphere. One cannot ice that the source Io-D is much less extended in CML than that displayed in Figure 2.

[19] It is possible to redraw the CML-Io phase diagram (see Figure 4) taking into consideration the active longitude ranges derived from Figure 3, the transformation from λ_a to Φ_{Io} being still obtained from equation (1). One can see in Figure 4 that the occurrence regions related to Io-A, Io-B, and Io-C have lost a corner while a large part of the Io-D source has disappeared in the range $0° < CML < 130°$. We have calculated the active longitude range for different values of the lead angle δ. The truncated occurrence regions in the CML-Io phase diagram remain unchanged compared with those in Figure 4, but the Jovian active zones are shifted in longitude. Table 2 lists the limits of the active longitude range for δ varying from 0° to 40°.

3. Constraints on the Opening Angle of the Emission Cone

[20] In section 2, we came across the difficulty of explaining that all sources are confined to their occurrence regions as usually observed in the CML-Io phase diagram. The choice of the Jovian magnetic field model (O6 in our study) allows us to determine which values are possible for the opening angle of the emission cone since the contour of the truncated source boxes in Figures 3 and 4 can be plotted as a function of the angle θ and the active IFT longitude. We consider calculating the angle θ sometimes from the magnetic field vector **B** and sometimes from the gradient of its modulus ∇B; in such a magnetized, low-density plasma the gradient of the refractive index is nearly parallel to the magnetic field intensity gradient, the magnetic field intensity gradient thus playing the role of an optical axis for the wave propagation. This dual analysis leads to constraint of the opening of the cone taking into account, at the same time, the propagation conditions of the waves (the angle measured from ∇B must be always greater than 90°) and the sense of circular polarization of the radiation (right- or left-handed depending on whether the angle θ measured from **B** is lower or greater than 90°). It should be remembered that the vectors **B** and ∇B are calculated at the point of the active field line where the gyrofrequency corresponds to the specified value of f. Finally, we consider two frequencies in our analysis: f = 16 MHz and f = 22 MHz, which properly characterize the observations coming from the southern and northern hemispheres.

Table 2. Active Longitude Range Versus Lead Angle

	North		South	
Lead Angle δ	λ_{min}	λ_{max}	λ_{min}	λ_{max}
0°	160°	265°	225°	294°
20°	140°	245°	205°	274°
40°	120°	225°	185°	254°

[21] The four Io-controlled sources are plotted as a function of θ and active IFT longitude in Figures 5, 6, and 7 for various values of the frequency f and lead angle δ. In any case, we have chosen $D_E = 0°$ for the Jovian declination of the Earth. A summary of these plots is presented in Table 3 where we report the source name, the observational parameters, the domains of angle with **B** and ∇B, the corresponding dominant polarization, the existence (or not) of a double polarization state, and the figure number.

[22] The main results are summarized below and have been obtained by combining Figures 5, 6, and 7. We consider three aspects: (1) the propagation, (2) the polarization, and (3) their combination.

3.1. Propagation Requirements

[23] The extension of the domain of the hollow cone half angles does not depend on the lead angle δ. However, the case $\delta = 20°$ seems to be the best case (see Figures 5 and 6) for the occurrence area of each source to have a half angle θ larger than 90°, allowing a wide domain of propagation. On the contrary, it is not the case for the two other values of δ (i.e., 0° and 40°) where nearly half of the occurrence areas are associated with hollow cones lower than 90° (with no possible propagation), this is especially true for Io-B and Io-D sources (see Figure 7).

3.2. Polarization Requirements

[24] We note that the occurrence area related to the half angle ranges of the hollow cone depends on the lead angle. The domains become larger when the lead angle δ increases, in particular, for the northern sources (see Figure 7). On the contrary, for $\delta = 40°$, the Io-D source displays a smaller occurrence area. We find that a lead angle of 20° is the most advantageous and adequate for the occurrence areas extension. Also, some sources show evidence of both right-hand (RH) and left-hand (LH) circular polarization (of about 50% RH and 50% LH), as one can see in Figure 7. So Io-B, Io-D exhibit a double circular polarization state for $\delta = 0°$, and Io-C exhibits a double circular polarization state for $\delta = 40°$.

3.3. Propagation and Polarization Conditions

[25] The vectors **B** and ∇B are not exactly parallel and they form an angle of a few degrees. On the other hand,

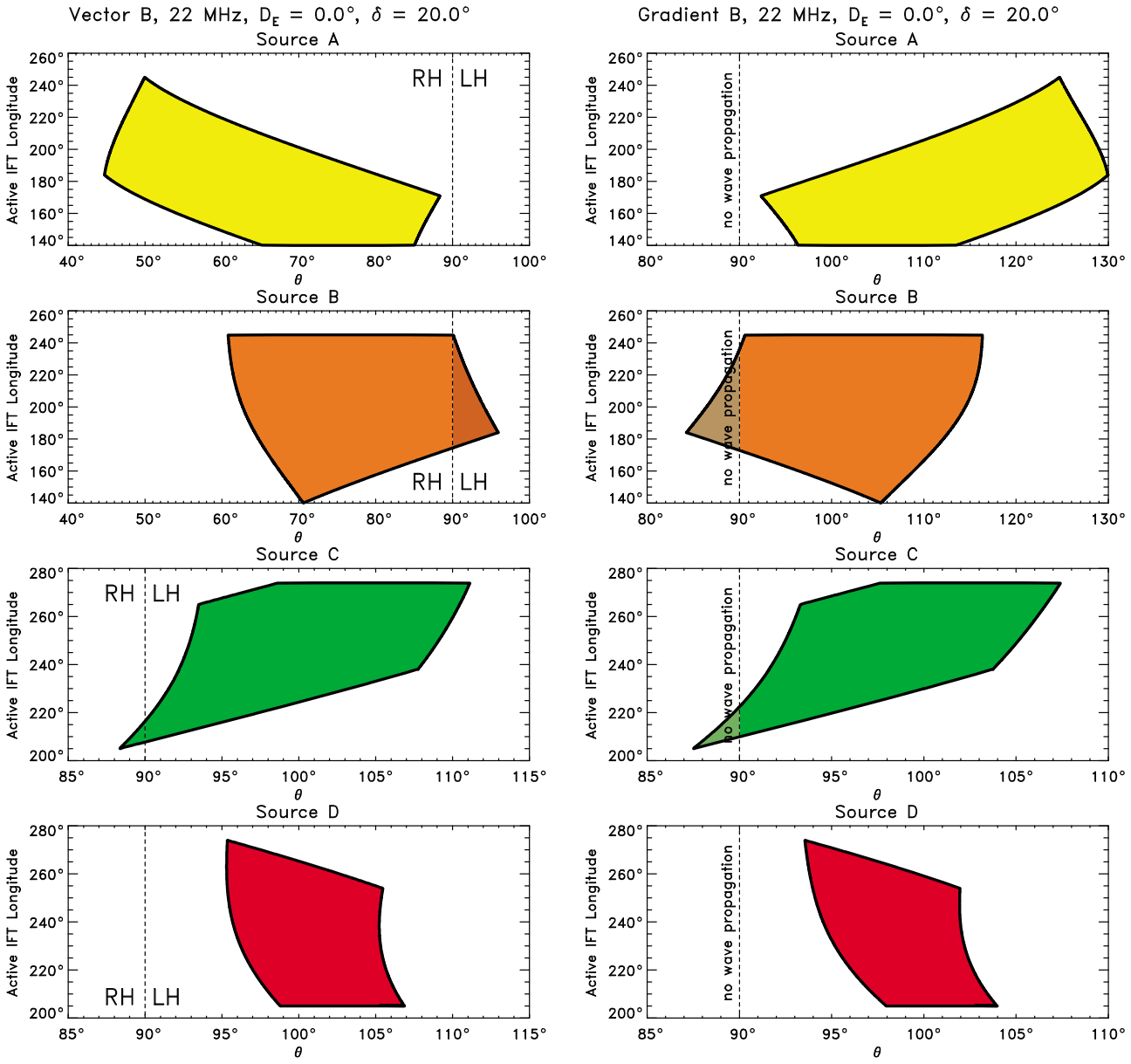

Figure 5. The four sources Io-A, Io-B, Io-C, and Io-D from Figures 3 and 4 are displayed as a function of the angle θ and the active Io flux tube longitude for a frequency of 22 MHz and a lead angle $\delta = 20°$. (left) The angle θ is measured from the magnetic field vector **B**; $\theta < 90°$ corresponds to a right-hand circular polarization while $\theta > 90°$ corresponds to a left-hand circular polarization. (right) The angle θ is measured from the gradient of the magnetic field modulus ∇B, so that the waves can propagate only for $\theta > 90°$. Such diagrams delimit the possible values of θ allowing a radio emission for the four sources.

these two vectors are approximately oriented in the same direction in the southern hemisphere, whereas they are oriented in opposite direction in the northern hemisphere. As a consequence, in Figures 5, 6, and 7, for a given emission cone, the values of θ measured relative to **B** and ∇B are nearly the same for the Io-C and Io-D sources, while they are distributed symmetrically around $\theta = 90°$ for Io-A and Io-B. The condition $\theta > 90°$ for the propagation is severe and considerably reduces the possible domains where a double polarization state may exist as was mentioned in section 3.2. The existence of an opposite circular polarization (e.g., LH for Io-A and Io-B, RH for Io-C and Io-D) depends very much on the value of δ (it is perceptible in Figure 7 for $\delta = 0°$ and 40°), for $\delta = 20°$ it is rather marginal (Figures 5 and 6).

3.4. Summary

[26] The comparison of the occurrence areas in Figure 5 (obtained for 22 MHz) and those in Figure 6 (obtained for 16 MHz) clearly shows that the half angle of the beaming cone does not depend very much on the emission frequency. Otherwise, the domain of the possible values for θ depends very much on the lead angle δ. According to Figure 7, there is no

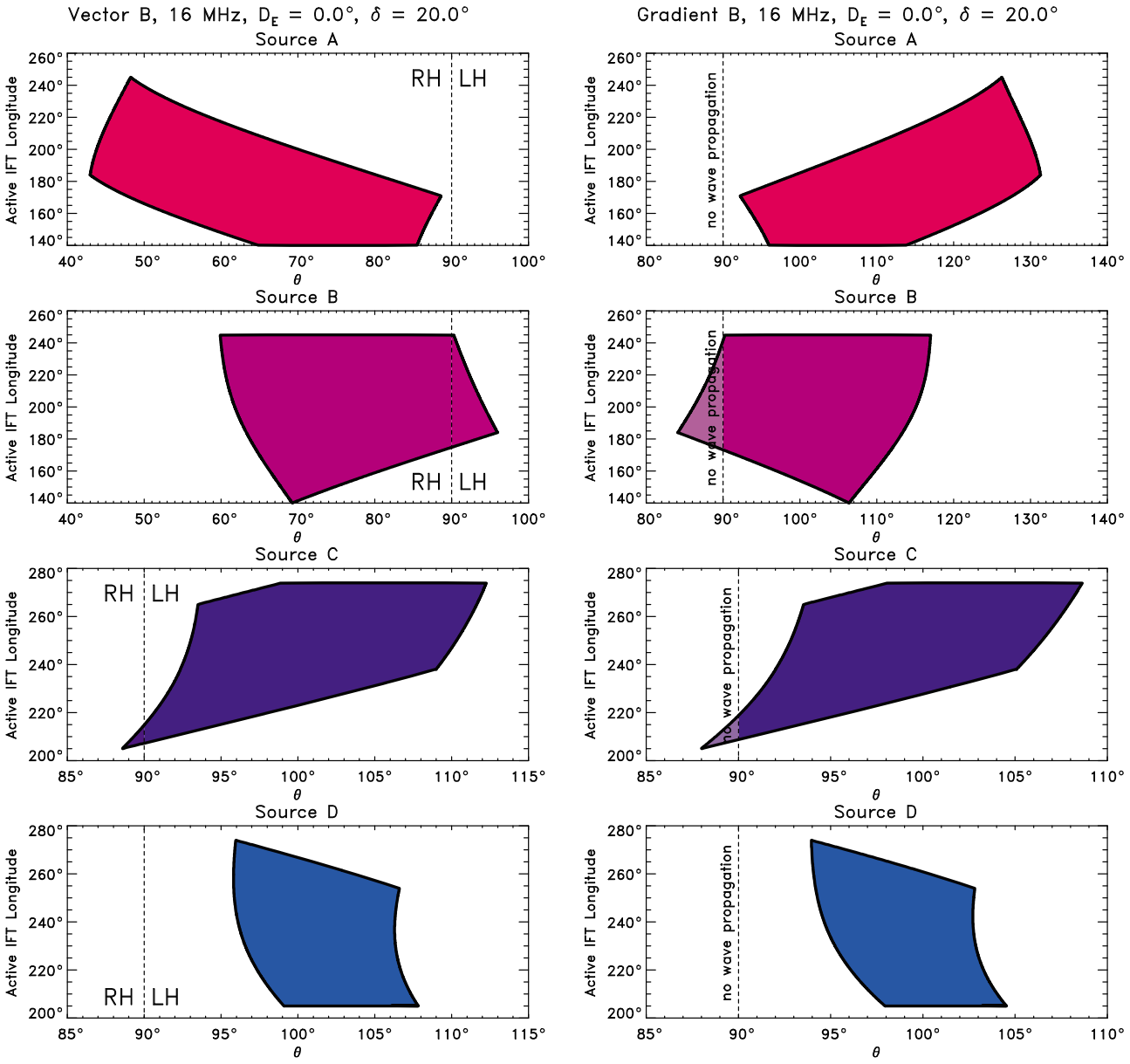

Figure 6. The same domains as in Figure 5 have been calculated for a frequency of 16 MHz (and the same value of the lead angle $\delta = 20°$). This shows that the domains of possible θ do not depend very much on the frequency.

common value of θ which simultaneously fits the four sources when $\delta = 0°$ or $\delta = 40°$. This is particularly obvious for Io-C and Io-D, for which the intersection exists only when $\delta \sim 20°$.

4. Discussion

[27] We investigate the occurrence probability of the Jovian decametric sources derived from a long-term observation (more than 50 years). The occurrence is usually displayed versus two observational parameters: the central meridian longitude and the phase of the satellite Io. The CML-Io phase diagram exhibits occurrence regions associated with DAM emissions and more particularly the Io-controlled radiation. In our analysis, we have attempted to find the adequate parameters which can lead to a good adjustment of the so-called occurrence regions using the active longitude model [see *Galopeau et al.*, 2004]. The key ingredients are the frequency and the lead angle, and the outcomes are the half angle of the hollow cone associated with the propagation and the polarization of the radio wave. In section 4, we address three main issues concerning the comparison between the modeled and observed CML-Io phase diagrams (section 4.1), the crucial role of the lead angle (section 4.2), and the necessity of integrating other possible processes which can increase the efficiency of the CMI mechanism (section 4.3).

4.1. Cyclotron Maser Instability and Concept of Hollow Cone

[28] We have found in our analysis the impossibility of associating radio sources from the same hemisphere to a

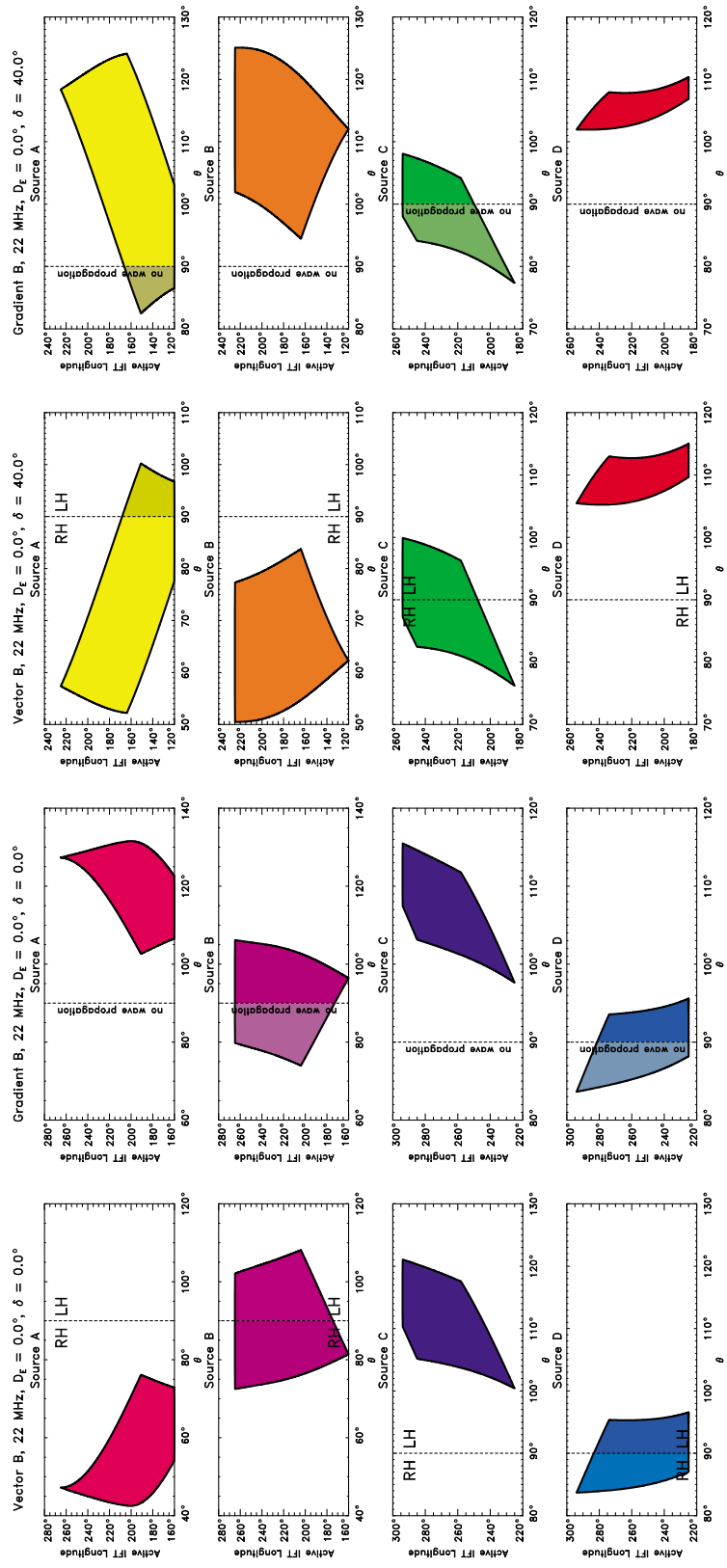

Figure 7. Domains of possible θ calculated for $\delta = 0°$ and $\delta = 40°$ at 22 MHz. These domains are very dependent on the value of the lead angle δ. For these two examples, no common value of θ simultaneously exists for Io-A, Io-B, Io-C, and Io-D.

Table 3. Summary of the Results[a]

Source	Parameter			Angle With ∇B	Angle With **B**	Dominant Polarization[b]	Double Polarization State	Figure
	δ	f	D_E					
Io-A	20°	22 MHz	0°	92°–130°	45°–88°	RH		5
Io-B	20°	22 MHz	0°	90°–115°	61°–96°	RH	Yes	5
Io-C	20°	22 MHz	0°	90°–107°	88°–111°	LH	Yes	5
Io-D	20°	22 MHz	0°	93°–104°	95°–107°	LH		5
Io-A	20°	16 MHz	0°	92°–132°	43°–88°	RH		6
Io-B	20°	16 MHz	0°	90°–116°	60°–96°	RH	Yes	6
Io-C	20°	16 MHz	0°	90°–109°	88°–108°	LH	Yes	6
Io-D	20°	16 MHz	0°	94°–104°	96°–107°	LH		6
Io-A	0°	22 MHz	0°	103°–132°	42°–77°	RH		7
Io-B	0°	22 MHz	0°	90°–105°	73°–90°	RH	Yes	7
Io-B	0°	22 MHz	0°	90°–105°	90°–107°	LH	Yes	7
Io-C	0°	22 MHz	0°	97°–115°	100°–121°	LH		7
Io-D	0°	22 MHz	0°	90°–95°	90°–96°	LH	Yes	7
Io-D	0°	22 MHz	0°	90°–95°	84°–90°	RH	Yes	7
Io-A	40°	22 MHz	0°	90°–124°	52°–100°	RH	Yes	7
Io-B	40°	22 MHz	0°	94°–125°	50°–84°	RH		7
Io-C	40°	22 MHz	0°	90°–98°	90°–100°	LH	Yes	7
Io-C	40°	22 MHz	0°	90°–98°	76°–90°	RH	Yes	7
Io-D	40°	22 MHz	0°	102°–110°	105°–115°	LH		7

[a]Domains of possible θ (half angle of emission cone) relative to ∇B (gradient of the magnetic field modulus) and relative to **B** (magnetic field vector), corresponding sense of dominant polarization and existence of a double polarization state deduced from Figures 5, 6, and 7. The results are sorted according to the values of the lead angle δ, the frequency f, and the Earth's declination D_E.

[b]For some extreme values of δ, there is no dominant polarization. Therefore, the RH and LH sources are indicated separately.

common opening angle of the hollow cone, this is particularly the case for Io-A and Io-B which are supposed to be emitted from the northern hemisphere. The southern hemisphere sources exhibit common half angles of the hollow cone which are such that the propagation and the polarization of the radio wave can be explained by CMI mechanism. Of course, we consider in our hypothesis that the emission diagram associated with the DAM radiation is a hollow cone. This assumption can be at the origin of the difficulty to reconcile observed and modeled source regions as deduced from the CML-Io phase diagram.

[29] Early ground-based observations have revealed that the hollow cone [*Dulk*, 1965] could explain the occurrence probability and spectral arc shapes related to Io-controlled emissions. Several authors have proposed models where each arc geometrically results from the rotation of sets of hollow cone beams emanating from a range of frequencies along an activated flux tube threaded by Io [*Carr et al.*, 1983]. However, two criticism should be addressed in relation to this concept of the hollow cone. First, the "arc shape" derived from the hollow cone is basically a geometrical construction without explicit reference to the cyclotron maser instability. Second, the combination of space and ground-based observations (frequency range from a few MHz to 40 MHz) led *Lecacheux et al.* [1998] to show that in the higher- and lower-frequency parts of DAM Io-controlled emissions a clear disagreement exists between the calculated beaming geometry and the observed spectral arc shapes. It appears that the "hollow cone" concept is a very idealistic and unlikely representation of the emission diagram. When comparing observed and modeled emission properties, one has to consider other effects like radio wave refraction, which occurs quasi systematically in the surrounding region of the radio source. The idea proposed by *Lecacheux et al.* [1998] seems to be more realistic and reasonable; a "radio horizon" concept is introduced taking into consideration the presence of radio wave refraction at grazing incidence above the planetary limb.

4.2. Crucial Role of the Lead Angle

[30] It is shown in our study that the lead angle is a key parameter when one tries to explain the active longitude derived from the CMI. We find that the occurrence probability source regions depend very much on the lead angle and almost not at all on other parameters like the frequency and the Jovicentric declination of the Earth.

[31] In this study, we notice that the occurrence areas grow when the lead angle increases, in particular, for the northern hemisphere sources (see Figure 7). However, at a lead angle equal to 40°, the Io-C and, in particular, Io-D sources have smaller occurrence areas. Also, when the lead angle is equal to zero (see Figure 7) one notes that for the Io-A and Io-D sources (1) only part of the emission can propagate and (2) the percentage of LH and RH polarized emissions is nearly similar. The optimal case is a lead angle of 20° where the sources from both hemispheres have satisfactory occurrence areas. Our result is in agreement with investigations by *Leblanc et al.* [1994] who suggested a geometrical method to derive in three dimensions the Io-controlled source locations. In particular, the authors found that a lead angle greater than 30° cannot be explained by the multibounce Alfven model proposed by *Gurnett and Goertz* [1981]. More recent investigations have considered a similar lead angle (equal to or smaller than 30°) in the modeling of parallel electric fields associated to Io-controlled Jovian arcs [*Su et al.*, 2003] or in the analysis of the Jovian DAM arc generation related to the Io flux tube [*Hess et al.*, 2008]. In the extreme case where the lead angle is equal to 0° or 40°, the behavior of the pairs {Io-B, Io-D} and {Io-A, Io-C} are similar, in particular, with regards to the polarization. This

may be due to the effect of Alfven waves excited by the satellite Io which simultaneously link two Io-controlled emissions, with opposite senses of polarization, generated in two hemispheres, despite the fact that their respective beaming cones may be different. Whatever the value of the lead angle δ, the frequency of observation does not seem to play any essential role in the location of the source regions in the CML-Io phase diagram (see Figure 6).

4.3. Sense of Circular Polarization

[32] As explained in section 3, we have the ability to derive the sense of circular polarization (LH or RH) depending on whether the angle θ measured from the magnetic field vector is greater or less than 90°. Our model correctly determines the position of the occurrence regions associated with the RH emissions (Io-A and Io-B) in the northern hemisphere and the LH emissions (Io-C) in the southern hemisphere, but the location of the Io-D source is not as good. The simplifying hypothesis of two northern sources 100% RH polarized and two southern sources 100% LH polarized is not fully correct. Actually, several authors have reported that the DAM emission is elliptically polarized for all sources [*Lecacheux et al.*, 1991; *Dulk et al.*, 1994; *Boudjada et al.*, 1995] and that both senses of polarization have been measured [*Boudjada and Genova*, 1991; *Leblanc et al.*, 1993b] in the case of Io-A (80% RH and 20% LH) and Io-C (60% LH and 40% RH). Only Io-B and Io-D sources appear in one single sense of elliptical polarization, right-handed and left-handed, respectively. These features cannot, of course, be achieved from our theoretical model because each source is supposed to be emitted from one hemisphere and to exhibit only one sense of circular polarization. Nevertheless, Figure 7 shows that, for a lead angle of 40°, some sources like Io-A and Io-C can have a double polarization state with percentages comparable to the observed ones (if the condition of propagation relative to ∇B is not taken into account).

[33] In fact, few investigations have been devoted to regularly monitor the sense of polarization of the Jovian DAM emissions at a large-frequency bandwidth. This means that our actual knowledge about occurrence domains in the CML-Io phase diagram is extremely limited. The main observation conditions have been discussed by *Galopeau et al.* [2004, 2007] who deal with the radio telescope properties (sensitivity, frequency bandwidth, and polarization of antennas), the terrestrial observation circumstances (e.g., a few hours before and after the local meridian), and the characteristics of the receivers (spectral resolutions and Stokes parameters measurements). Regular space observations of the Jovian DAM emissions by the Wind WAVES experiment helped to fill a gap in observations as reported by *Kaiser and Garcia* [1997]. The use of polarization measurements involving ground-based and Wind satellite observations [*Lecacheux et al.*, 1998; *Aubier et al.*, 2000] allows us to find that the RH and LH source regions have different behaviors in the CML-Io phase diagram. The extensions of those occurrence regions in the northern and southern hemispheres depend on the central meridian longitude and the Io phase, respectively. These features have been reported by Figure 2 of *Boudjada and Genova* [1991] and Figure 6 of *Aubier et al.* [2000] where the authors combined LH and RH polarization measurements of the Jovian DAM emissions observed during the same time period. This means that the electron fluxes at the origin of those Io-controlled emissions vary mainly as the intensity of Jupiter's internal magnetic field varies (this is especially the case for the radiations coming from the northern hemisphere) and moderately depends on the position of Io in its orbit.

5. Conclusion

[34] Through a series of three papers we have made an attempt at understanding the location of the Io-controlled sources in the CML-Io phase diagram. The first two papers of the series [*Galopeau et al.*, 2004, 2007] were dedicated to the search for observational parameters (e.g., frequency, lead angle, opening angle of the beaming cone) allowing us to reproduce the observed CML-Io phase diagram within the framework of a radio emission generated by the CMI and beamed in an axisymmetrical hollow cone. That study brought out the existence of an active longitude anchored in Jupiter's magnetic field and directly linked to the efficiency of the CMI. In this paper, we have adopted a reverse procedure; we have derived the active longitude range from the location of the sources in the CML-Io phase diagram with the main assumption that the radiation is beamed in an axisymmetrical hollow cone. Nevertheless, we have not made any preconceived suppositions about the mechanism generating the radio emission. Finally, our investigations have led to a modeled CML-Io phase diagram where the source regions present a thickness. This model rests on two essential assumptions which might be questioned: a common active longitude range (linked to the efficiency of the emission mechanism) and a radiation beamed in a hollow cone.

[35] For the modeled occurrence diagram, we consider in this study two fundamental physical parameters: the propagation and the polarization of the radio wave. These two factors allow us to derive the active longitude ranges of the Io-controlled sources and the corresponding theoretical occurrence regions. It follows that the lead angle has a significant effect on the selection of the propagation conditions and on the limit between RH and LH polarization states. An optimal case where the modeled and observed occurrence regions are nearly similar, has been found for a lead angle $\delta = 20°$. Smaller or greater values of δ cannot lead to any acceptable adjustment of the observation occurrence.

[36] Despite the concordance of the modeled and observed diagrams (in particular for Io-A and Io-B) one has to note that the polarization and the area of the occurrence regions of the southern hemisphere sources are trickier. In a future study, it may be relevant to deeply modify some hypotheses of the model; in particular, introducing a nonconstant electron distribution function at Io's orbit and a more complex beaming cone. One has to consider other effects like the electron scattering in the Io plasma torus and variations of the particle acceleration in Io's ionosphere [*Zaitsev et al.*, 2006]. However, it seems that the behaviors of the southern and northern sources are not alike despite a common generation mechanism. Other processes favoring the northern sources have to be taken into consideration, solar wind control for instance.

[37] **Acknowledgments.** Masaki Fujimoto thanks Kazumasa Imai and another reviewer for their assistance in evaluating this manuscript.

References

Aubier, M. G., and F. Genova (1985), A catalogue of the high frequency limit of the Jovian decameter emission observed by Voyager, *Astron. Astrophys. Suppl. Ser.*, *61*, 341–351.

Aubier, A., M. Y. Boudjada, P. Moreau, P. H. M. Galopeau, A. Lecacheux, and H. O. Rucker (2000), Statistical studies of Jovian decameter emissions observed during the same period by Nançay decameter array (France) and WAVES experiment aboard Wind spacecraft, *Astron. Astrophys.*, *354*, 1101–1109.

Boudjada, M. Y., and F. Genova (1991), The left-hand polarization sense of the Jovian decameter radiation, *Astron. Astrophys. Suppl. Ser.*, *91*, 453–467.

Boudjada, M. Y., and Y. Leblanc (1992), The variability of Jovian decametric radiation from 1978 to 1988, *Adv. Space Res.*, *12*, 95–98, doi:10.1016/0273-1177(92)90382-8.

Boudjada, M. Y., H. O. Rucker, and P. H. Ladreiter (1995), The Io-C Jovian decameter emissions, *Astron. Astrophys.*, *303*, 255–264.

Burke, B. F., and K. L. Franklin (1955), Observations of a variable radio source associated with planet Jupiter, *J. Geophys. Res.*, *60*, 213–217.

Carr, T. D., and M. D. Desch (1976), Recent decametric and hectometric observations of Jupiter, in *IAU Colloquium 30: Jupiter: Studies of the Interior, Atmosphere, Magnetosphere and Satellites*, pp. 693–737, Univ. of Ariz. Press, Tucson, Ariz.

Carr, T. D., M. D. Desch, and J. K. Alexander (1983), Phenomenology of magnetospheric radio emissions, in *Physics of the Jovian Magnetosphere*, edited by A. J. Dessler, pp. 226–284, Cambridge Univ. Press, New York.

Connerney, J. E. P. (1992), Doing more with Jupiter's magnetic field, in *Planetary Radio Emissions III*, edited by H. O. Rucker, S. J. Bauer, and M. L. Kaiser, pp. 13–33, Austrian Acad. of Sci., Vienna.

Connerney, J. E. P. (1993), Magnetic fields of the outer planets, *J. Geophys. Res.*, *98*(E10), 18,659–18,679, doi:10.1029/93JE00980.

Connerney, J. E. P., M. H. Acuña, N. F. Ness, and T. Satoh (1998), New models of Jupiter's magnetic field constrained by the Io flux tube footprint, *J. Geophys. Res.*, *103*(A6), 11,929–11,940, doi:10.1029/97JA03726.

Dulk, G. A. (1965), Io-related radio emission from Jupiter, *Science*, *148*, 1585–1589.

Dulk, G. A., Y. Leblanc, and A. Lecacheux (1994), The complete polarization state of Io-related radio storms from Jupiter: A statistical study, *Astron. Astrophys.*, *286*, 683–700.

Galopeau, P. H. M., M. Y. Boudjada, and H. O. Rucker (2004), Evidence of Jovian active longitude: 1. Efficiency of cyclotron maser instability, *J. Geophys. Res.*, *109*, A12217, doi:10.1029/2004JA010459.

Galopeau, P. H. M., M. Y. Boudjada, and H. O. Rucker (2007), Evidence of Jovian active longitude: 2. A parametric study, *J. Geophys. Res.*, *112*, A04211, doi:10.1029/2006JA011911.

Genova, F., and M. G. Aubier (1987), High frequency limit and visibility of the non-Io and Io-dependent Jovian decameter radio emission, *Astron. Astrophys.*, *177*, 303–309.

Genova, F., P. Zarka, and A. Lecacheux (1989), Jupiter decametric radiation, in *Time Variable Phenomena in the Jovian System*, *NASA Spec. Publ. Ser.*, vol. 494, edited by M. J. S. Belton, R. A. West, and J. Rahe, pp. 156–174, NASA, Washington, D. C.

Grodent, D., B. Bonfond, J. Gérard, A. Radioti, J. Gustin, J. T. Clarke, J. Nichols, and J. E. P. Connerney (2008), Auroral evidence of a localized magnetic anomaly in Jupiter's northern hemisphere, *J. Geophys. Res.*, *113*, A09201, doi:10.1029/2008JA013185.

Gurnett, D. A., and C. K. Goertz (1981), Multiple Alfven wave reflections excited by Io origin of the Jovian decametric arcs, *J. Geophys. Res.*, *86*(A2), 717–722.

Hess, S., F. Mottez, P. Zarka, and T. Chuss (2008), Generation of the Jovian radio decametric arcs from the Io flux tube, *J. Geophys. Res.*, *113*, A03209, doi:10.1029/2007JA012745.

Imai, K., J. J. Riihimaa, F. Reyes, and T. D. Carr (2002), Measurement of Jupiter's decametric radio source parameters by the modulation lane method, *J. Geophys. Res.*, *107*(A6), 1081, doi:10.1029/2001JA007555.

Imai, M., K. Imai, C. A. Higgins, and J. R. Thieman (2008), Angular beaming model of Jupiter's decametric radio emissions based on Cassini RPWS data analysis, *Geophys. Res. Lett.*, *35*, L17103, doi:10.1029/2008GL034987.

Kaiser, M. L., and L. N. Garcia (1997), Jupiter's low frequency radio spectrum: Filling in the gaps, in *Planetary Radio Emissions IV*, edited by H. O. Rucker, S. J. Bauer, and A. Lecacheux, pp. 17–24, Austrian Acad. of Sci., Vienna.

Leblanc, Y., A. Gerbault, L. Denis, and A. Lecacheux (1993a), A catalogue of Jovian decametric radio observations from January 1988 to December 1990, *Astron. Astrophys. Suppl. Ser.*, *98*, 529–546.

Leblanc, Y., F. Bagenal, and G. A. Dulk (1993b), The Jovian left hand polarized radiation, *Astron. Astrophys.*, *276*, 603–613.

Leblanc, Y., G. A. Dulk, and F. Bagenal (1994), On Io's excitation and the origin of Jupiter's decametric radiation, *Astron. Astrophys.*, *290*, 660–673.

Lecacheux, A. (2000), The Nançay decameter array: A useful step towards giant, new generation radio telescopes for long wavelength radio astronomy, in *Radio Astronomy at Long Wavelengths*, *Geophys. Monogr. Ser.*, vol. 119, edited by R. G. Stone et al., pp. 321–328, AGU, Washington, D. C.

Lecacheux, A., A. Boischot, M. Y. Boudjada, and G. A. Dulk (1991), Spectra and complete polarization state of two, Io-related, radio storms from Jupiter, *Astron. Astrophys.*, *251*, 339–348.

Lecacheux, A., M. Y. Boudjada, H. O. Rucker, J. L. Bougeret, R. Manning, and M. L. Kaiser (1998), Jovian decameter emissions observed by the Wind/WAVES radioastronomy experiment, *Astron. Astrophys.*, *329*, 776–784.

Su, Y., R. E. Ergun, F. Bagenal, and P. A. Delamere (2003), Io-related Jovian auroral arcs: Modeling parallel electric fields, *J. Geophys. Res.*, *108*(A2), 1094, doi:10.1029/2002JA009247.

Treumann, R. A. (2006), The electron cyclotron maser for astrophysical application, *Astron. Astrophys. Rev.*, *13*, 229–315, doi:10.1007/s00159-006-0001-y.

Wu, C. S., and L. C. Lee (1979), A theory of the terrestrial kilometric radiation, *Astrophys. J.*, *230*, 621–626.

Zaitsev, V. V., V. E. Shaposhnikov, and H. O. Rucker (2003), Electron acceleration in the ionosphere of Io, *Astron. Rep.*, *47*, 701–708, doi:10.1134/1.1601639.

Zaitsev, V. V., V. E. Shaposhnikov, and H. O. Rucker (2005), Electron acceleration at the Io's ionosphere and origin of active longitudes in the Jovian decametric radio emission, *Adv. Space Res.*, *36*, 2106–2109, doi:10.1016/j.asr.2005.03.045.

Zaitsev, V. V., V. E. Shaposhnikov, and H. O. Rucker (2006), Dependence of the Io-related decametric radio emission of Jupiter on the central meridian longitude and Io's "active" longitudes, *Astron. Astrophys.*, *454*, 669–676, doi:10.1051/0004-6361:20054450.

M. Y. Boudjada, Space Research Institute, Austrian Academy of Sciences, Schmiedlstr. 6, A-8042 Graz, Austria. (mohammed.boudjada@oeaw.ac.at)

P. H. M. Galopeau, LATMOS, Université Versailles Saint-Quentin-en-Yvelines, CNRS, INSU, IPSL, Quartier des Garennes, 11 Blvd. d'Alembert, F-78280 Guyancourt, France. (patrick.galopeau@latmos.ipsl.fr)